AD-A047 810 NAVAL RESEARCH LAB WASHINGTON D C F/G 4/1
THE ZONALLY AVERAGED CIRCULATION OF THE MIDDLE ATMOSPHERE.(U)
OCT 77 M SCHOEBERL, D STROBEL
UNCLASSIFIED NRL-MR-3590 SBIE-AD-E000 063 NL

| OF |
AD
A047810

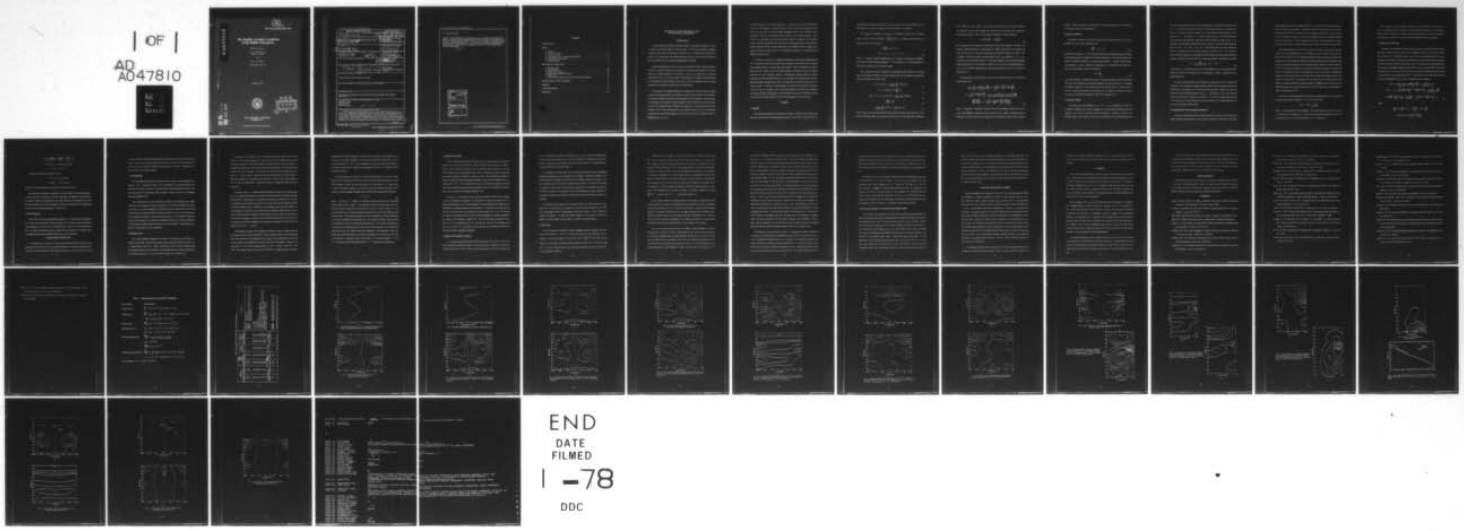

END
DATE
FILMED
1 -78
DDC

(12) NW

NRL Memorandum Report 3590

The Zonally Averaged Circulation of the Middle Atmosphere

MARK R. SCHOEBERL

Science Applications Inc.
McLean, Va. 22101

and

DARRELL F. STROBEL

Plasma Physics Division

October 1977

NAVAL RESEARCH LABORATORY
Washington, D.C.

SECURITY CLASSIFICATION OF THIS PAGE (When Data Entered)

REPORT DOCUMENTATION PAGE

READ INSTRUCTIONS BEFORE COMPLETING FORM

1. REPORT NUMBER: NRL Memorandum Report 3590
2. GOVT ACCESSION NO. (14)
3. RECIPIENT'S CATALOG NUMBER: NRL-MR-3590

4. TITLE (and Subtitle): (6) THE ZONALLY AVERAGED CIRCULATION OF THE MIDDLE ATMOSPHERE
5. TYPE OF REPORT & PERIOD COVERED: (9) Interim report on a continuing NRL Problem
6. PERFORMING ORG. REPORT NUMBER

7. AUTHOR(s): (10) M. Schoeberl and D. Strobel
8. CONTRACT OR GRANT NUMBER(s): (16) F52551

9. PERFORMING ORGANIZATION NAME AND ADDRESS: Naval Research Laboratory, Washington, D.C. 20375 (12) 43 p.
10. PROGRAM ELEMENT, PROJECT, TASK AREA & WORK UNIT NUMBERS: NRL Problem A03-23, Project NASC WF52-551-713

11. CONTROLLING OFFICE NAME AND ADDRESS (11)
12. REPORT DATE: Oct[illegible]977 (17)
13. NUMBER OF PAGES: 42

14. MONITORING AGENCY NAME & ADDRESS (if different from Controlling Office): (18) SBIE (19) AD-E000 063
15. SECURITY CLASS. (of this report): UNCLASSIFIED
15a. DECLASSIFICATION/DOWNGRADING SCHEDULE

16. DISTRIBUTION STATEMENT (of this Report)

Approved for public release; distribution unlimited.

17. DISTRIBUTION STATEMENT (of the abstract entered in Block 20, if different from Report)

18. SUPPLEMENTARY NOTES

This research was sponsored by the Naval Air Systems Command Agency under Subtask WF52-551-713.

19. KEY WORDS (Continue on reverse side if necessary and identify by block number)

Newtonian cooling
Rayleigh friction
Middle atmosphere
OXYGEN
OZONE

20. ABSTRACT (Continue on reverse side if necessary and identify by block number)

(U) The steady state, zonally averaged circulation of the middle atmosphere (15-125 km) is studied with a quasigeostrophic, numerical model that explicitly includes a self-consistent calculation of solar radiative heating due to O_2 and O_3 absorption, Newtonian cooling, Rayleigh friction, tropopause boundary conditions based on climatological averages, and the effects of vertically propagating planetary waves. We find the direct, radiatively driven pole to pole circulation at solstice is sufficient to account for the cold summer mesopause and warm isothermal winter mesosphere with associated

(Continued)

DD FORM 1 JAN 73 1473 EDITION OF 1 NOV 65 IS OBSOLETE
S/N 0102-LF-014-6601

SECURITY CLASSIFICATION OF THIS PAGE (When Data Entered)

251 950

20. Abstract (Continued)

zonal jets of realistic magnitude. The climatological heat and momentum fluxes associated with planetary wave number 2 have a negligible effect on the mean circulation. With planetary wave number 1 no steady state solution could be obtained due to the formation of easterlies and hence critical layers in the winter mesosphere. We also find that the radiative heating associated with secondary peaks in the O_3 density at the mesopause could render the polar mesopause region convectively unstable.

OZONE

CONTENTS

THE ZONALLY AVERAGED CIRCULATION OF THE MIDDLE ATMOSPHERE

I. INTRODUCTION

In recent years there has been considerable interest in stratospheric chemistry as a result of concern about pollution effects on the ozone layer. In the lower and middle stratosphere transport processes affect the ozone density distribution as a consequence of its long chemical lifetime. The motion field of the middle atmosphere is thus not only of intrinsic interest but plays an important role in our chemical understanding of this region.

Vertically propagating planetary waves forced in the troposphere provide an important dynamical mechanism to couple the stratosphere and troposphere. The reflection and transmission of these ultra-long waves are strongly dependent on the structure of zonal wind jets centered near the stratopause (Schoeberl and Geller, 1977). Further progress in understanding such fundamental dynamical processes in the stratosphere as sudden warmings and their effects on the lower atmosphere require a thorough knowledge of the dynamical processes that control the polar night jet.

The dynamics of the middle atmosphere is often described in terms of a zonally averaged circulation and perturbations from this average. The latter include a variety of wave phenomena which are principally controlled by linear processes and thus amenable to accurate quantative simulations. The symmetric (zonally averaged) circulation depends on the nonlinear eddy statistics of the middle atmosphere through the divergences of the heat and momentum fluxes associated with the wave perturbations and on solar radiative heating. The lack of information on eddy statistics has hampered progress since the initial attempt of Leovy (1964) to model the

Manuscript submitted July 13, 1977.

symmetric circulation of the middle atmosphere. At solstice Leovy showed that radiative forcing by ozone absorption of sunlight would drive a pole to pole mean circulation that could explain the polar night jet, the cold summer mesosphere and the warm, isothermal, winter mesosphere. These are the essential observed features of the middle atmosphere. Since Leovy's work considerably more data have become available for comparison with theoretical models. Also important advances have been made in the parameterization of infrared radiative cooling (Dickinson, 1973a), accurate representation of the differential radiative heating due to insolation (Park and London, 1974), and photochemical acceleration of thermal relaxation (Blake and Lindzen, 1973).

In this paper we show that it is possible to numerically simulate certain essential features of the symmetric circulation with accurate input parameters and representation of the eddy heat divergence based on the above mentioned advances. While our approach and model is similar to Leovy's (1964), we solve the resultant equations numerically and relax a number of constraints that Leovy imposed to produce a mathematically tractable problem for analytic techniques. We allow Newtonian cooling to vary with height and latitude whereas our only adjustable parameter, Rayleigh friction, varies with height only for lack of information on its latitudinal variation. In addition, we have attempted to include the contributions of planetary waves with zonal wave numbers 1 and 2 to the local divergences of the eddy heat and momentum fluxes by explicitly computing their wave amplitude with the model of Schoeberl and Geller (1977) which is based on Matsuno's (1970, 1971) formulation for ultra-long waves.

II. MODEL

A. Equations

The approximate equations that describe the symmetric circulation of the middle atmosphere can be derived with the scaling arguments used by Leovy (1964), (cf. Holton, 1975). As

our equations are essentially those obtained by Leovy (1964) with only slight differences in the final formulation, we merely summarize the salient assumptions and arguments.

The equilibrium atmosphere is assumed to be motionless, hydrostatic, and in radiative balance. With the vertical coordinate $z = ln\left(\frac{p_o}{p}\right)$, where p_o is a reference pressure taken to be 100mb, the basic state equations are

$$\frac{\partial < \phi >}{\partial z} = R < T > \tag{1}$$

$$< H > \simeq < \alpha > < T > + < b > \tag{2}$$

where $< >$ denotes a globally averaged quantity (i.e. zonally and meridionally averaged), α and b are the Newtonian cooling coefficients, T is the temperature, ϕ is the geopotential, R is the dry air gas constant, and H is the solar heating.

The symmetric circulation is described by meteorological fields denoted by an overbar that are the difference between the zonally averaged fields and the globally averaged fields. The relevant equations are (Leovy, 1964)

$$- k_r \bar{u} + 2\Omega \bar{v} \sin\theta = \frac{1}{a \cos^2 \theta} \frac{\partial}{\partial \theta} (\overline{u'v'} \cos^2\theta) \tag{3}$$

$$- k_r \bar{v} + 2\Omega \bar{u} \sin \theta + \frac{1}{a} \frac{\partial \bar{\phi}}{\partial \theta} = 0 \tag{4}$$

$$S\bar{w} + [< \alpha > + \alpha_{pc}] \bar{T} = \bar{H} - \frac{1}{a \cos \theta} \frac{\partial}{\partial \theta} (\overline{v'T'} \cos \theta) \tag{5}$$

$$\frac{\partial \bar{\phi}}{\partial z} = R\bar{T} \tag{6}$$

$$\frac{1}{a \cos \theta} \frac{\partial}{\partial \theta} (\bar{v} \cos \theta) + \frac{1}{p} \frac{\partial}{\partial z} (p\bar{w}) = 0 \tag{7}$$

where $\bar{u}$ and $\bar{v}$ are the eastward (westerly) and northward (southerly) wind velocities, θ is latitude, a is the earth's radius, Ω is the earth's rotation rate, k_r is the Rayleigh friction coefficient,

and $\bar{w} = \frac{dz}{dt}$, the "vertical velocity". The last term on the RHS of Eqs. (3) and (5) represents the divergences of the zonally averaged eddy momentum and heat fluxes, due to large scale quasi-stationary planetary waves. S is the globally averaged static stability defined as

$$S = \frac{R < T >}{c_p} + \frac{\partial < T >}{\partial z} \tag{8}$$

$\bar{H}$ is the differential solar heating due principally to the earth-sun geometry. The term $\alpha_{pc} \bar{T}$ represents differential heating or cooling due to O_3 density perturbations that accelerate the thermal relaxation rate in the upper stratosphere and mesosphere (Blake and Lindzen, 1973). An effective Newtonian cooling or thermal relaxation rate, α_{eff}, is defined as $< \alpha > + \alpha_{pc}$. The Eulerian time derivatives in Eqs. (3) - (5) have been neglected since the annual oscillation frequency associated with the symmetric circulation is much less than the damping frequency, α_{eff}. To avoid numerical difficulties which arise near the equator the term $k_r \bar{v}$ has been retained in Eq. (4).

Eliminating $\bar{u}$ and $\bar{v}$ between Eqs. (3), (4), and (7) and $\bar{w}$ from (5) and (7), we arrive at a single equation for $\bar{\phi}$

$$\frac{k_r}{\cos\theta} \frac{\partial}{\partial \theta} \left[\frac{\cos\theta}{\gamma^2 + \sin^2\theta} \frac{\partial \bar{\phi}}{\partial \theta} \right] + e^z \frac{\partial}{\partial z} \left[\frac{e^{-z} (2\Omega a)^2 \alpha_{eff}}{SR} \frac{\partial \bar{\phi}}{\partial z} \right]$$

$$= e^z \frac{\partial}{\partial z} \left[\frac{e^{-z} (2\Omega a)^2 \bar{H}}{S} \right] + \frac{1}{2\Omega a^2} \frac{1}{\cos\theta} \frac{\partial}{\partial \theta} \left[\frac{1}{\sin\theta} \left\{ \frac{1}{\cos\theta} \frac{\partial}{\partial \theta} \left[\frac{\cos\theta}{\sin\theta} \right.\right.\right.$$

$$\left.\left.\left. \left[\overline{\frac{\partial \phi'}{\partial \lambda} \frac{\partial \phi'}{\partial \theta}} \right] + e^{-z} \frac{\partial}{\partial z} \left[\frac{e^{-z} (2\Omega a)^2}{SR} \left[\overline{\frac{\partial \phi'}{\partial \lambda} \frac{\partial \phi'}{\partial z}} \right] \right] \right\} \right] \tag{9}$$

where $\gamma = \frac{k_r}{2\Omega}$ and λ is longitude. The eddy flux terms are discussed in Section 2E. Eq. (9) is an elliptic differential equation and may be solved by any number of standard numerical techniques. We used a form of Crout reduction which is described in most texts on numerical

methods. Adequate convergence was obtained with vertical grid spacing of 0.45 scale heights and horizontal spacing of 5 latitude degrees.

B. Boundary Conditions

The boundary condition at the north and south poles is obtained from Eq. (4) by the requirement that u and v must vanish there; thus

$$\frac{\partial \bar{\phi}}{\partial \theta} \Big|_{\theta = \pm \pi/2} = 0 \tag{10}$$

Along the lower boundary ($z = 0$) we define a geopotential distribution based upon the observational statistics given by Taljaard et al. (1968) and Labitzke et al. (1972) for the southern and northern hemispheres, respectively. Along the upper boundary ($\sim$ 125km) we assume radiative equilibrium is valid by increasing the magnitude of α_{eff} to include thermal conduction as well as 15μ CO_2 radiation. Thus Eq. (5) reduces to

$$\bar{T} = \frac{\bar{H}}{\alpha_{eff}} \tag{11}$$

at the upper boundary. Unfortunately H cannot be precisely determined without knowledge of $\bar{T}$ since the local densities of the absorbing constituents O_2 and O_3 depend on $\bar{T}$. Accordingly we assume initially that $\bar{T} = 0$, compute $\bar{H}$, and solve Eqs. (9) and (11). Using the new $\bar{T}$ values, we update $\bar{H}$ and repeat the above process until convergence is achieved. In practice only two or three iterations are required to obtain 0.2K convergence for $\bar{T}$.

C. Newtonian Cooling

The Newtonian cooling coefficient, $\alpha_{eff} = <\alpha> + \alpha_{pc}$, is a global function, while the b coefficient is defined to be a function of height only. The atmospheric cooling rate due to IR emission by CO_2 and O_3 has been accurately calculated by Dickinson (1973a) for the 30-100km region. Above 70km the accuracy of the Newtonian cooling representation breaks

down but is still retained for lack of a better representation. We estimate the asymptotic value of $<\alpha>$ at 95km to be the CO_2 cooling rate in its fundamental band at 15μ and above this level by the thermal conduction relaxation rate. Below 30km we adopt Trenbeth's (1973) values for $<\alpha>$. The resultant $<\alpha>$ profile is displayed in Fig. 1. The ozone photochemical acceleration of the Newtonian cooling rate is based on Blake and Lindzen (1973). For an atmosphere with odd oxygen chemistry the thermal relaxation rate for local, small-scale perturbations is $1400\ (<H> + \bar{H})\ (<T> + \bar{T})^{-2}$ above 40km where the recent NBS recommended rate coefficients have been adopted (Hampson and Garvin, 1975). In the real atmosphere where odd hydrogen and odd nitrogen chemistry affects ozone concentrations Blake and Lindzen concluded that the above value of α_{pc} should be reduced by approximately one half to

$$\alpha_{pc} = \frac{700}{(<T> + \bar{T})^2}\ (<H> + \bar{H}) \tag{12}$$

Above 70km, α_{pc} is asymptotically set to zero. The applicability of Eq. (12) to global scale perturbations, where the *UV* transmissitivity of the atmosphere is altered, is questionable as discussed in Section 3C.

We achieve radiative balance in the atmosphere as represented by Eq. (2) in the following manner. Since the globally averaged temperature profile is fairly well known and the major contributions to solar heating, $<H>$, can be accurately computed, we choose $<b>$ in Eq. (2) to obtain the required radiative balance with the $<\alpha>$ profile shown in Fig. 1. This procedure is more accurate than any attempt now to calculate $<b>$ from first principles and then infer $<T>$ from Eq. (2). We have found that the derived values for $<b>$ below 70km are in accord with the Dickinson (1973a) results.

D. Parameterization of the Atmospheric Heating Rate

In order to numerically simulate the middle atmosphere circulation, accurate and computationally efficient parameterizations of solar radiative heating by O_3 absorption in the Hartley

region, Huggins bands, and the Chappius bands and by O_2 absorption in the Schumann-Runge bands and continuum are required. A particularly convenient parameterization was introduced by Lindzen and Will (1973) who noted that if O_3 absorption cross sections are either constant or have an exponential variation over individual wavelength intervals, the atmospheric heating rate can be expressed as the sum of simple analytic formulas. We have adopted this parameterization scheme and only summarize the results here, details may be found in Strobel (1976).

Below approximately 80 km the $O(^3P)$ formed by O_3 and O_2 dissociation recombines quickly and the actual heating rate of the atmosphere is the total photon energy absorbed. Above 80 km the $O(^3P)$ may be transported significantly before recombining, and the actual heating rate is the net heating rate (defined as the energy absorbed minus the chemical energy stored by the dissociated products) plus the chemical energy released by locally recombining $O(^3P)$. To a good first approximation we can estimate the actual heating rate by summing the *total* (net + chemical) O_3 and the *net* O_2 heating rates. We are only interest in the differential heating rate and the results of Park and London (1974) indicate that chemical recombination heating is at most 5K day $^{-1}$ above 80 km and that transport of $O(^3P)$ tends to minimize the differential chemical recombination heating and render it negligible when compared to the net differential heating. Our heating rates agree well with their results when the comparison is made at the same density levels.

In Table 1 the *total* heating rates for O_3 and the *net* heating rates for O_2, Q_i, are tabulated by spectral region in units of ergs cm $^{-3}$s $^{-1}$ and are related to H by

$$< H > + \overline{H} = \frac{1}{\rho\, c_p} \sum_i Q_i$$

where ρ is the mass density of the atmosphere. The column densities of O_2 and O_3 (N_2 and N_3, respectively) are computed by an 8 point Gaussian quadrature integration scheme. The number densities of O_2 and O_3 are denoted by n_2 and n_3, respectively.

The time scale for motions under consideration is long compared to a day and only the diurnally averaged heating rate is required. We have adopted approximation # 4 of Cogley and Borucki (1976) to accurately and quickly evaluate average heating rates. We have obtained an overall accuracy of better than ± 10 percent when compared with "exact" calculations.

E. Computation of Eddy Fluxes

The eddy heat and momentum fluxes in equation (9) are computed by solving a separate perturbation equation governing planetary wave propagation, similar to that derived by Schoeberl and Geller (1977). Stationary planetary waves with zonal wavenumbers one and two are observed to have sufficient amplitude in the stratosphere at mid latitudes to account for greater than 90% of the eddy statistics (van Loon et al., 1973). The steady state wave perturbations are calculated on a grid staggered along the mid points of the mean circulation grid. We take the Rayleigh friction, k_r, to be the same for both wave and mean flow geopotentials but Newtonian cooling for the wave is approximated by $<\alpha>$ since planetary waves are important only in the winter hemisphere where α_{pc} is small. The planetary wave equation is:

$$(i\bar{\omega}m + k_r)\left[\frac{1}{\cos\theta}\frac{\partial}{\partial\theta}\frac{\cos\theta}{\gamma^2 + \sin^2\theta}\frac{\partial\psi'}{\partial\theta} - \frac{m^2}{\cos^2\theta\sin^2\theta}\psi'\right]$$

$$+ (i\bar{\omega}m + <\alpha>)\left[\frac{(2\Omega a)^2}{S}\frac{\partial^2\psi'}{\partial z^2} + \frac{(2\Omega a)^2 A}{S}\psi'\right] + \frac{im\psi'}{\cos\theta\sin^2\theta}\frac{\partial\bar{q}}{\partial\theta}$$

$$+ \frac{(2\Omega a)^2}{S}\frac{\partial <\alpha>}{\partial z}\left(\frac{1}{2} + \frac{1}{2S}\frac{\partial S}{\partial z}\right)\psi' + \frac{\partial <\alpha>}{\partial z}\frac{(2\Omega a)^2}{S}\frac{\partial\psi'}{\partial z} = 0 \qquad (13)$$

where

$$\frac{\partial\bar{q}}{\partial\theta} = \cos\theta\left\{2(\Omega + \bar{\omega}) - \frac{\partial\bar{\omega}}{\partial\theta^2} + 3\tan\theta\frac{\partial\bar{\omega}}{\partial\theta} - \right.$$

$$\left.(2\Omega a)^2\sin^2\theta\, e^{z}\frac{\partial}{\partial z}\left[\frac{e^{-z}}{S}\frac{\partial\bar{\omega}}{\partial z}\right]\right\};$$

$$A = \frac{3}{4}\frac{1}{S^2}\left[\frac{\partial S}{\partial z}\right]^2 + \frac{1}{2S}\left[\frac{\partial S}{\partial z} - \frac{\partial^2 S}{\partial z^2}\right] + \frac{1}{4};$$

$$\bar{\omega} = \bar{u}/a\cos\theta;\ m = \text{zonal wavenumber}$$

$$\psi' = \phi' e^{-z/2} S^{-1/2}.$$

The boundary conditions on equation (13) are:

$$\psi' = 0,\quad z = 16\ (\sim 125\ \text{km})$$

$$\psi' = F(\theta),\quad z = 0\ (\sim 16\ \text{km})$$

where $F(\theta)$ is the climatological forcing given by van Loon et al. (1973).

The steady state contribution of planetary wave eddy fluxes on the mean circulation is evaluated iteratively by computation of the wave amplitude in the presence of the zonal flow at that iteration followed by the adjustment of the mean circulation to the divergence of the eddy fluxes just computed. This iteration procedure is continued until both the wave amplitude and the mean circulation adjustments decrease to less than 5%.

F. Model Atmosphere

CIRA (1972) was the model atmosphere adopted for $<T>$ and the O and O_2 mixing ratios. The O_3 density distribution is based on Krueger (1973). Other O_3 density distributions were considered above 75 km and will be discussed below in Section 3F. The latitudinal variation of O_3 density along constant pressure surfaces has been neglected in the present model since differential solar heating depends primarily upon earth-sun geometry.

III. THE SOLSTITIAL CIRCULATION

A principal goal of this study is to assess the quantitative effects of various physical processes on the mean circulation of the middle atmosphere. We proceed by comparing calculations where these processes have been added or deleted one at a time to see how the total

circulation is altered. The most sensitive indicator of the mean circulation is the zonal wind at solstice. In each test calculation described in this section we show only the mean zonal wind profile but give other diagnostic variables at selected altitudes in Table II. All diagnostic variables are shown for the final calculations.

A. The Heating Rate

The perturbation heating rate, $\bar{H}$, at solstice is shown in Figure 2, while the globally averaged rate, $<H>$, is illustrated in Figure 3. In the stratosphere O_3 absorption dominates the heating rate whereas O_2 absorption is responsible for the large heating rate above 90 km. Note that to first order, $\bar{H}$ is antisymmetric about the equator. There is, however, a non-negligible symmetric component of $\bar{H}$.

Leovy (1964) showed that the antisymmetric component of the heating drives a single, direct pole to pole circulation cell with upward motion in the summer hemisphere and downward motion in the winter hemisphere. Conversely, symmetric heating forces two cells with upward motion over equatorial regions and downward motion at the pole. Coriolis torques act on the meridional circulation to produce strong zonal winds. For antisymmetric heating the zonal wind jets are easterly in the summer hemisphere and westerly in the winter hemisphere, whereas symmetric heating produces westerly jets in both hemispheres. The heating shown in Figure 2 will yield features of both components.

B. Rayleigh Friction

The principal adjustable coefficient in this model is the Rayleigh friction coefficient, k_r. There is, unfortunately, no self consistent theory which can be used to estimate its value. Leovy (1964) adopted a value of $k_r \sim 0.1$ day $^{-1}$ which Green (1972) criticized as being too large. To illustrate the sensitivity of the zonal jets to the Rayleigh friction we present calculations for three constant values of k_r^{-1}: 30, 15 and 7.5 days in Figure 4a, b, c, respectively.

In the absence of Rayleigh friction, the meridional circulation vanishes if the vertical velocity is zero at the lower boundary, as is the case here, and the temperature field is strictly in radiative equilibrium. Under these conditions a large meridional temperature gradient is produced which generates a vertical shear in the zonal wind, consistent with the thermal wind equation. This case is illustrated in Fig. 4a where the strength of the jets increases with altitude up to $\sim$ 110 km. Since k_r is small, but finite the wind contours close at high altitudes indicating the presence of a weak pole to pole circulation. The zonal wind structure shown in Fig. 4a bears little resemblance to observations reported in Murgatroyd (1969) and CIRA (1965, 1972).

For larger values of k_r a stronger vertical field develops in response to the external heating in the stratosphere and reduces the meridional temperature graidient by adiabatic processes. More specifically, upward motion at the summer pole decreases the temperature from its radiative equilibrium value and downward motion over the winter pole raises the temperature above its radiative equilibrium value. Consequently the stratospheric zonal wind shear weakens. In the mesosphere the strength of the vertical motions are sufficiently large to reverse the meridional temperature gradient imposed by radiative balance and thus close the zonal wind contours below the mesopause. In Figs. 4b and 4c this result is demonstrated. The jet maxima occur between 60 and 80 km in agreement with observations, although the jet intensities are too great in Fig. 4b with $k_r^{-1} = 15$ days.

The temperature gradient at the mesopause as indicated in Table 2 is a good indicator of the magnitude of the vertical motion field. Another important feature which distinguishes these three calculations is the separation of the jet maxima in each hemisphere into two lobes with one peak in the mesosphere and the other in the lower thermosphere. Associated with these lobes are the two major heating regimes: O_3 and O_2 insolation, respectively. CIRA (1965, 1972) suggest easterly winds above the mesopause in equatorial regions (where our

quasigeostrophic model is inadequate) and westerlies at mid latitudes in both hemispheres. Observations for this region are difficult to obtain because of atmospheric tidal motions. Calculations by Dickinson et al. (1977) of the thermospheric circulation also indicate the presence of jets similar to those shown in Figure 4c with amplitudes of 80-120 ms $^{-1}$ peaking at 120 km and about 60° latitude.

From the results shown in Figure 4 it is clear that large values of $k_r \geq 0.1$ day $^{-1}$, are required above the stratopause to produce the observed wind and temperature structure. For the lower stratosphere, Lindzen (private communication, 1977) has noted that k_r^{-1} values of 10 to 15 days would severely dampen the quasi-biennial oscillation (Holton and Lindzen, 1971). These two constraints suggest a Rayleigh friction profile with the following functional form:

$$k_r = k_o \, e^{z/c} \tag{14}$$

where $c = 4.43$ and $k_o^{-1} = 40$ days. The computed zonal wind structure with this Rayleigh friction profile is shown in Figure 5. The agreement between the observed zonal wind structure and this case is better than was achieved with a constant k_r value (cf. Figure 4c). Note also from Table 2 that the computed mesopause temperatures are also in better agreement with the observations. The warmer temperatures in the winter mesosphere and cooler temperatures in the summer mesosphere are associated with a more vigorous meridional circulation above the stratopause as a result of the enhanced Rayleigh friction. Vertical motion fields generated by heating at the stratopause increase in intensity with altitude because k_r and ν are small and cannot "short circuit" the w field by continuity considerations in the stratosphere. Other functional forms for Rayleigh friction are not ruled out by Equation (14). We find only two criteria to be important in generating realistic mean fields in the middle atmosphere: (a) that $k_r^{-1} \geq 40$ days in the lower stratosphere and (b) $k_r^{-1} \sim 10$ days above the stratopause.

C. Photochemical Damping

We now include photochemical acceleration of Newtonian cooling with the rate given by equation (12) and retain the exponential k_r profile. The results of this calculation are shown in Figure 6. From a comparison of Figures 5 and 6 it is apparent that the easterly jet in the summer stratosphere is more strongly affected with a 15 ms $^{-1}$ reduction at the peak. Additionally, the summer stratopause temperature is lowered by about 10K. Photochemical acceleration effectively reduces the meridional temperature gradient in the summer hemisphere since α_{pc} is proportional to $<H> + \overline{H}$. As expected, the zonal jet in the summer mesosphere is now less intense than observed which may indicate that smaller values of k_r are appropriate for that region or that α_{pc} has been overestimated by equation (12).

The rate for α_{pc} was derived for local, small scale perturbations where the UV transmissivity of the atmosphere is independent of the perturbation (cf. Blake and Lindzen, 1973). For global scale perturbations with vertical scales greater than the atmospheric scale height, the UV transmissivity is significantly affected for optical depths $\geqslant 1$. Estimates for the latter case indicate that at unit optical depth, the perturbation to the heating rate is zero (i.e. $\alpha_{pc} = 0$) because the change in the heating rate due to local O_3 density perturbations is precisely cancelled by the change in UV transmissivity (Strobel, 1977). Thus for global scale perturbations the rate given by Eq. (12) is appropriate only for the optically thin case where the heating rate and hence α_{pc} are small. As a consequence we have neglected the photochemical acceleration of Newtonian cooling in subsequent calculations.

D. Realistic Lower Boundary Conditions

In our previous calculations the lower boundary condition was $\phi(\theta, 0) = 0$. We now include a geopotential perturbtion defined by observational statistics compiled by Taljaard et al. (1969) and Labitzke et al. (1972). Figure 7 presents calculations for $\overline{u}$, $\overline{v}$, $\overline{w}$, and $\overline{T}$ when sum-

mer is in the Southern hemisphere, while Figure 8 is for winter. The $\bar{u}$ and $\bar{w}$ fields exhibit the most noticable asymmetries and thus the $\bar{v}$ and $\bar{T}$ fields are not presented for the later calculation. We have used the exponential Rayleigh friction profile but have neglected photochemical acceleration of Newtonian cooling.

It is apparent from these figures that the tropopause height field induces considerable hemispherical asymmetry into the stratosphere and mesosphere. Particularly remarkable is the upward extension of tropospheric westerlies into the stratospheric easterly jet in Figure 7a. No such extension occurs in the equivalent calculations for summer in the Northern hemisphere (cf. Figure 8a). Overall, realistic lower boundary conditions have a major effect only below 50 km where the westerlies are intensified in both winter hemispheres, the summer easterlies in the Southern hemisphere are weakened, and the Northern hemisphere summer easterlies are intensified.

The relatively weak influence at the boundary forcing on the mean circulation is consistent with the analytic solutions of equation (9) which have been studied by Leovy (1964) and Longuet-Higgins (1968). Longuet-Higgins denotes these solutions as Type 7 solutions to Laplace's tidal equation. The equivalent depths associated with the solutions are small and negative so boundary effects will decay rapidly with height as our results indicate.

E. Eddy Fluxes

We now consider the influence of vertically propagating stationary planetary waves with zonal wave numbers $m = 1$ and $m = 2$. The vertical structure of these disturbances is controlled by the meridional gradient of the potential vorticity, $\frac{\partial \bar{q}}{\partial \theta}$, and the strength and the shape of the polar night jet (Matsuno, 1970; Schoeberl and Geller, 1977). The function $\frac{\partial \bar{q}}{\partial \theta} \cos \theta^{-1}$ is shown in Figure 9 for the zonal wind structure presented in Figure 7, where winter is in the Northern hemisphere.

A change in the sign of $\frac{\partial \bar{q}}{\partial \theta}$ is a necessary condition for wave instability (Charney and Stern, 1962). The negative region above 80 km in the winter mesosphere on the right hand side of Figure 9 results from negative shear above the jet maximum as discussed previously by Dickinson (1973b) and Simmons (1974). They suggest planetary waves may be baroclinically unstable in this region. Simmons (1977) has also examined the possibility of such instability in the summer mesosphere as a result of positive shear in the stratospheric easterlies. The growth of unstable waves in either region is opposed by the large radiative and photochemical damping rates so no firm conclusion has been reached on the importance of unstable waves in the mesosphere. In order to compute the influence of vertically propagating planetary waves in steady state equilibrium with the mean circulation we suppress instabilities by giving $\frac{\partial \bar{q}}{\partial \theta} \cos \theta^{-1}$ a positive value of 10^{-5} s $^{-1}$ where a sign change occurs.

For an arbitrarily large wave amplitude forced at 100 mb there is no guarantee that the iterative scheme will converge. The modification of the mean flow by wave flux convergences may enhance these fluxes at the next iteration and thus lead to a numerically non-convergent sequence. For example, if easterlies appear in the region dominated by the wave field, convergence will be unlikely due to critical level effects (Dickinson, 1969; Matsuno, 1971). Note also that we have not included the displacement of the equatorial easterlies by the quasi biennial oscillation so that possible critical level effects have been neglected at low latitudes.

For $m = 1$ we could not obtain numerical convergence using climatological wave amplitudes given by van Loon et al. (1973). After the first iteration, easterly winds appeared near the winter pole mesopause and the iterative procedure diverged due to the build up of eddy heat and momentum flux convergence at the critical level. Numerical convergence was obtained when the wave amplitude was uniformly reduced to 1/3 of the climatological value at the lower boundary to a peak amplitude of 45 gpm. With reduced wave amplitude, the $m = 1$

eddy exerted a negligible influence on the mean circulation since its flux convergence is proportional to $(\phi')^2$. To illustrate the impact of the $m = 1$ eddy with the full climatological amplitude at 100 mb we show the meteorological fields after the first iteration when the eddy fluxes were added as heat and momentum sources in Fig. 10. We have found that the convergence of northward eddy heat fluxes is strongest at about 85 km and poleward of 75°N with secondary convergence occurring at 30 km poleward of 65°N associated with local maxima of wave amplitude (Figure 10e). The convergence of zonal momentum flux occurs at approximately the same altitudes and latitudes with an additional divergence occuring at 65 km poleward of 65°N. The primary eddy forcing of the mean flow appears to be the northward heat flux convergence which sets up a local circulation cell near the winter pole (Figure 10c, d) and generates the strong easterlies there (Figure 10a). The intensity of the polar night jet is reduced by $\sim$10% as a result of eddy heat and momentum flux convergences, with the heat flux convergence at 30 km being the dominant contributor. In the winter polar mesosphere the temperature has increased by $\sim$70K due to the $m = 1$ eddy. This temperature extreme is, of course, not observed and the circulation pattern shown in the upper parts of Figure 10 should be regarded as illustrative. The points demonstrated by this calculations are (a) a reduction of the jet strength by stratospheric eddy heat convergence and (b) the appearance of easterly winds in the upper mesosphere due to eddy heat convergence in the mesosphere. This later region might be regarded as an initiation point for critical levels which could later progress downward to generate sudden stratospheric warmings (Matsuno, 1971; Holton, 1976).

The penetration of the polar night jet by the $m = 1$ planetary wave shown in Figure 10e is consistent with calculations made by Schoeberl and Geller (1977) who showed that the $m = 1$ wave is generally not trapped except for very strong jets. The numerical divergence of the iteration method may also indicate that the stratospheric $m = 1$ wave never attains a steady solution but will vacillate in amplitude throughout the winter. Vacillation behavior of planetary waves has been examined by Holton and Mass (1976). The reduced amplitude which we

found would give convergence may be related to the minimum amplitude required for such stratospheric vacillations; however, we note that our minimum amplitude is about three times smaller than that deduced by Holton and Mass. This discrepancy is probably due to the fact that the winter mean zonal wind profile used by Holton and Mass does not decrease above 60 km.

For planetary wave $m = 2$ convergence could be obtained for climatological forcing. The wave amplitude for $m = 2$ is shown in Figure 11; note that this wave is trapped in the lower stratosphere with a smaller amplitude than $m = 1$ (Figure 10e). The effect of $m = 2$ on the mean circulation is negligible as might be expected from the weaker wave amplitude. The trapping of this wave by the polar night jet is also consistent with calculations made by Matsuno (1970) and Schoeberl and Geller (1977). Clearly, for $m = 2$, the eddy heat flux convergence will be largest in the lower stratosphere, but the mean circulation associated with this convergence is so weak that less than a 1% reduction in the jet amplitude occurs.

F. The Local Static Stability as a Function of Ozone Density Profiles

In the course of this investigation we discovered that the radiative heating associated with certain ozone profiles generated perturbation equilibrium temperatures sufficiently large in the polar mesopause region to drive the local static stability negative. This is a necessary condition for convection and invalidates the use of a globally averaged static stability in our model. Figure 12 shows three ozone profiles tested by our model: Profile I based on Hays and Roble (1973); Profile II extrapolated from Krueger (1973) and used in our previous calculations; and Profile III, an intermediate profile. Profile I yields locally large heating regions ~ 2 scale heights below the Schumann-Runge band heating region. The rapid variation of $<\alpha>$ and its small value combined with the large altitude variation of $\bar{H}$ produce a radiative equilibrium temperature profile with a super-adiabatic lapse rate. Such variations are also present for

Profiles II and III but with smaller amplitude and generate only sub-adiabatic lapse rates. We note that if Profile I were produced by ozone photochemistry and our choice of the Newtonian cooling rate is appropriate, then the convection and associated turbulence generated by this large-scale thermal forcing may be self-sustaining since the chemical and convection time constants are comparable ($\sim$10 min). As a result of this convection, the summer polar mesopause temperature could be lowered sufficiently to condense water vapor and form noctilucent clouds. The convection would also generate the vigorous vertical motion required by Reid (1975) in his model of these ice clouds.

IV. THE MEAN CIRCULATION AT EQUINOX

Using the Rayleigh friction profile given by Eq. (14), lower boundary geopotential fields from Taljaard et al. (1969) and Labitzke et al. (1972) for April conditions, and $\alpha_{pc} = 0$, we have computed the mean circulation at equinox which is shown in Fig. 13. The perturbation heating rate (Fig. 13a) is symmetric about the equator as expected with peak heating rate of $\sim$3 K day $^{-1}$ at the equator and maximum cooling rate of $\sim$11K day $^{-1}$ at the poles in the ozone layer. The slight asymmetry in the zonal jets results from the asymmetrical lower boundary conditions. Both the temperature and zonal wind profiles are in good agreement with observations (CIRA, 1965, 1972); however, Table 2 indicates that the calculated jets occur at a lower altitude. The meridional circulation pattern illustrates the double cell structure characteristic of the symmetric heating at equinox: rising motion over the equatorial region and sinking motion at the poles. We conclude that the extratropical mean circulation at equinox and solstice are driven by the same physical processes. Equatorial motions are not adequately described by our quasigeostrophic model and no attempt is made to compare computed equatorial motions with observations.

At midlatitudes, Dickinson (1969) has shown that vertically propagating planetary waves undergo strong radiative damping at equinox and the extratropical effects of planetary wave

eddy stresses are regarded as negligible. Rayleigh friction may thus be weaker during equinox which would raise the location of the calculated zonal jets and remove the discrepancy noted previously.

V. SUMMARY

Using a numerical quasigeostrophic model we conclude that the essential features of the zonally averaged, extratropical circulation can be adequately understood if Dickinson's (1973a) Newtonian cooling rate is the appropriate thermal relaxation rate and friction is described by the Rayleigh coefficient given in Eq. (14). In particular we find the direct, radiatively driven pole to pole circulation at solstice is sufficient to account for the cold summer mesopause and the warm isothermal winter mesosphere with associated zonal jets of realistic magnitude, thus confirming Leovy's (1964) original hypothesis.

The climatological heat and momentum fluxes associated with planetary wave number 2 have a negligible effect on the mean circulation. For planetary wave $m = 1$ we could not obtain a steady state contribution of eddy forcing to the mean circulation given the observed climatological wave amplitude at the tropopause. Instead we suggest that the stratospheric response to this magnitude of $m = 1$ forcing will be a vacillation behavior as previously discussed by Holton and Mass (1976). According to our calculations the threshold amplitude for this response is only 1/3 of the climatological forcing, a factor of 3 less than the threshold obtained by Holton and Mass. Below the threshold value the $m = 1$ planetary wave has a negligible effect on the mean circulation of the middle atmosphere.

Our computations suggest that the thermal damping rate in the vicinity of the stratopause cannot substantially exceed Dickinson's Newtonian cooling rate. The photochemical acceleration of the thermal damping rate calculated by Blake and Lindzen (1973) is inapplicable to the global, large vertical scale motion considered here because UV transmissivity effects are important.

Another interesting result of our calculations is the inference that secondary peaks in the O_3 density near the mesopause will thermally force the summer polar mesopause region to be convectively unstable and significantly lower its temperature. This increases the possibility of water vapor condensation to form ice clouds. In addition convection will supply the vigorous vertical motion required by Reid (1975) in his model of noctilucent clouds.

ACKNOWLEDGEMENTS

The authors would like to thank Professor R. S. Lindzen for useful comments and Harry S. van Loon for providing planetary wave data. The major part of this research was supported by the Naval Air Systems Command with additional support from the Upper Atmospheric Research Office of the National Aeronautics and Space Administration.

REFERENCES

Blake, D. and R.S. Lindzen, 1973: Effect of photochemical models on calculated equilibria and cooling rates in the stratosphere, *Mon. Wea. Rev.*, **101**, 783-802.

Charney, J.G. and M.E. Stern, 1962: On the stability of internal baroclinic jets in a rotating atmosphere. *J. Atmos. Sci.*, **19**, 159-172.

CIRA 1965: *COSPAR International Reference Atmosphere*, Amsterdam, North-Holland, 313 pp.

CIRA 1972: *COSPAR International Reference Atmosphere*, Berlin, Akedemie-Verlag, 450 pp.

Cogley, A.C. and W.J. Borucki, 1976: Exponential Approximation for Daily Average Solar Heating or Photolysis. *J. Atmos. Sci.*, **33**, 1347-1356.

Dickinson, R.E., 1969: Vertical propagation of planetary Rossby waves through an atmosphere with Newtonian cooling. *J. Geophys. Res.*, **74**, 929-938.

Dickinson, R.E., 1973a: Method of parameterization for infrared cooling between altitudes of 30 and 70 kilometers, *J. Geophys. Res.*, **78**, 4451-4457.

Dickinson, R.E., 1973b: Baroclinic instability of an unbounded zonal shear flow in a compressible atmosphere. *J. Atmos. Sci.*, **30**, 1520-1527.

Dickinson, R.E., E.C. Ridley, and R.G. Roble, 1977: Meridional Circulation in the Thermosphere II. Solstice conditions *J. Atmos. Sci.*, **34**, 178-192.

Green, J.S.A., 1972: Large Scale motion in the upper stratosphere and mesosphere: an evaluation of data and theories. *Phil. Trans. Roy. Soc. Lond.*, **271**, 577-583.

Hampson, R.F., Jr., and D. Garvin, 1975: Chemical kinetic and photochemical data for modelling atmospheric chemistry. NBS Tech. Note. 866, 113 pp.

Hays, P.B. and R.G. Roble, 1973: Observation of mesospheric ozone at low latitudes. *Planet. Space Sci.*, **21**, 273-279.

Holton, J.R., 1975: *The Dynamic Meteorology of the Stratosphere and Mesosphere Meteor. Mon.*, **15**, Boston, Amer. Met. Soc., 216 pp.

Holton, J.R., 1976: A semi-spectral numerical model for wave-mean flow interactions in the stratosphere: applications to sudden stratospheric warnings. *J. Atmos. Sci.*, **33**, 1639-1649.

Holton, J.R. and R.S. Lindzen, 1972: An updated theory for the quasi-biennial cycle of the tropical stratosphere. *J. Atmos. Sci.*, **32**, 712-719.

Holton, J.R. and C. Mass, 1976: Stratospheric vacillation cycles. *J. Atmos. Sci.*, **33**, 2218-2225.

Krueger, A.J., 1973: The mean ozone distribution from several series of rocket soundings to 52 km at latitudes from 58°S to 64°N. *Pure and Appl. Geophys.*, **106-108**, 1272-1280.

Labitzke, K. and Collaborators, 1972: *Climatology of the Stratosphere in the northern hemisphere Part I, Heights, temperatures and geostrophic resultant wind speeds at 100, 50, 30, and 10 mb, Meteorol. Abhaudl.* **100**, 6 pp.

Leovy, C.B., 1964: Simple models of thermally driven mesospheric circulations. *J. Atmos. Sci*, **21**, 327-341.

Lindzen, R.S. and D.I. Will, 1973: An analytic formula for heating due to ozone absorption, *J. Atmos. Sci.*, **30**, 513-515.

Longuet-Higgins, M.S., 1968: The eigenfunctions of Laplaces' tidal equations over a sphere. *Phil. Trans. Roy. Soc. London*, **A262**, 511-607.

Matsuno, T., 1971: A dynamic model of the stratospheric sudden warming, *J. Atmos. Sci.*, **28**, 1479-1492.

Matsuno, T., 1970: The vertical propagation of stationary planetary waves in the winter northern hemisphere, *J. Atmos. Sci.*, **27**, 871-883.

Murgatroyd, R.J., 1969: The structure and dynamics of the stratosphere. *The Global Circulation of the Atmosphere*, G.A. Corby, Ed., London, Roy. Meteor. Soc., 159-195.

Park, J.H. and J. London, 1974: Ozone photo chemistry and radiative heating of the middle atmosphere. *J. Atmos. Sci.*, **31**, 1898-1961.

Reid, G.C., 1975: Ice clouds at the summer polar mesopause. *J. Atmos. Sci.*, **32**, 523-535.

Schoeberl, M.R. and M.A. Geller, 1977: A calculation of the structure of stationary planetary waves in winter, *J. Atmos. Sci.*, **34**, in press.

Simmons, A.J., 1974: Baroclinic instability at the winter stratopause. *Quart. J. Roy. Meteor. Soc.* **100**, 531-540.

Simmons, A.J., 1977: Baroclinic instability in the summer mesosphere, *Quart. J. Roy. Meteor. Soc.*, **103**, 211-215.

Strobel, D.F., 1976: Parameterization of the atmospheric heating rate from 15 to 120 km due to O_2 and O_3 absorption of solar radiation. NRL Memo Rept. 3398, Naval Research Laboratory, Washington D.C.

Strobel, D.F., 1977: Photochemical-Radiative Damping and Instability in the Stratosphere, *Geophys. Res. Lett.*, submitted.

Taljaard, J.J., H. van Loon, H.L. Crutcher and R.L. Jenne, *Climate of the upper air, Part 1 - Southern hemisphere*, NAVAIR 50-1C-55, 3 pp.

Trenbeth, K.E., 1973: Global model of the general circulation of the atmosphere below 75 km with animal heating cycle. *Mon. Wea. Rev.*, **101**, 306-322.

van Loon, H., R.L. Jenne, and K. Labitzke 1973: Zonal harmonic standing waves, *J. Geophys. Res.*, **78**, 4463-4471.

Table 1 – Parameterization of the Atmospheric Heating Rate

Spectral Region	Parameterization*
Chappius bands	$\frac{Q_c}{n_3} = 1.05 \times 10^{-15} \exp(-2.85 \times 10^{-21} N_3)$
Huggins bands	$\frac{Q_{Hu}}{n_3} = \frac{1}{N_3}\{4.66 \times 10^{3} - 7.8 \times 10^{2} \exp(-1.77 \times 10^{-19} N_3)$ $-3.88 \times 10^{3} \exp(-4.22 \times 10^{-18} N_3)\}$
Hartley region	$\frac{Q_{Ha}}{n_3} = 4.8 \times 10^{-14} \exp(-8.8 \times 10^{-18} N_3)$
Herzberg continuum	$Q_{Hz} = (9.9 \times 10^{-21} n_2 + 7.35 \times 10^{-15} n_3) \times$ $\exp(-6.6 \times 10^{-24} N_2 - 4.9 \times 10^{-18} N_3)$
Schumann-Runge bands	$\frac{Q_{SRB}}{n_2} = \frac{1}{0.67 N_2 + 3.44 \times 10^{9} N_2^{1/2}}$ If $N_2 < 10^{18}\ cm^2$, $\frac{Q_{SRB}}{n_2} = 2.43 \times 10^{-19}$
Schumann-Runge continuum	$\frac{Q_{SRC}}{n_2} = \frac{1}{N_2}\{0.98 \exp(-2.9 \times 10^{-19} N_2) - 0.55 \exp$ $(-1.7 \times 10^{-18} N_2) - 0.43 \exp(-1.15 \times 10^{-17} N_2)\}$

*Q_i is in ergs cm $^{-3}$ s $^{-1}$, n_i in cm^{-3}, N_i in cm $^{-2}$.

Table 2 — Observations and Representative Diagnostic Variables for Model Calculations

$\bar{u}$ (ms^{-1}) 70km Max. Value		Solstice $\bar{T}$ (K) 86 km Pole Values		$\bar{v}$ (ms^{-1}) 54 km Max Value	$\bar{w}\times 7.0\times 10^5$ cm (cms^{-1}) 55 km Pole Values		Model Description	
Winter H.	Summer H.	Winter H.	Summer H.		Winter H.	Summer H.		
80	-60	> 240	< 170	–	–	–	Observations	Murgatroyd (1969)
80	-62	272	139	–	–	–	Observations	CIRA (1965), (80 km for $\bar{T}$, Summer H. temperature taken for July)
108	-60	211	140	–	–	–	Observations	CIRA (1972), (80 km for $\bar{T}$, Summer H. temperature taken for July, Pole values at 70°N, S)
109	-75	177	186	0.73	-0.03	0.05	k_r^{-1} = 30 days	
92	-65	197	171	1.03	-0.06	0.08	k_r^{-1} = 15 days	
70	-52	205	162	1.35	-0.13	0.13	k_r^{-1} = 7.5 days	
79	-55	225	145	1.12	-0.08	0.09	k_r defined by eq. (14)	
76	-38	222	152	0.90	-0.08	0.06	k_r defined by eq. (14); photochemical damping added	
83	-46	226	148	1.12	-0.11	0.004	k_r defined by eq. (14) plus boundary conditions for Winter, Northern Hemisphere	
82	-55	226	145	1.15	-0.10	0.008	k_r defined by eq. (14) plus boundary conditions for Summer, Northern Hemisphere	
73	-46	257	148	1.10	-0.06	0.004	Winter, Northern Hemisphere plus m = 1 zonal harmonic	
81	-46	223	148	1.12	-0.12	0.004	Winter, Northern Hemisphere plus m = 2 zonal harmonic	
		Equinox						
$\bar{u}$ Max. Value 70 km		$\bar{T}$ at 50 km		$\lvert\bar{v}\rvert$ at 60 km	$\bar{w}$ at 60 km			
Southern H.	Northern H.	Equator	Northern H.		Equator	Northern H.		
45	45	273	285	–	–	–	Observations	CIRA (1965) (data for separate hemispheres not given)
40	40	275	267				Observations	CIRA (1972) (data for separate hemispheres not given)
31	29	271	247	0.38	0.017	-0.16	k_r defined by equation (14) plus boundary conditions for April, N.H.	

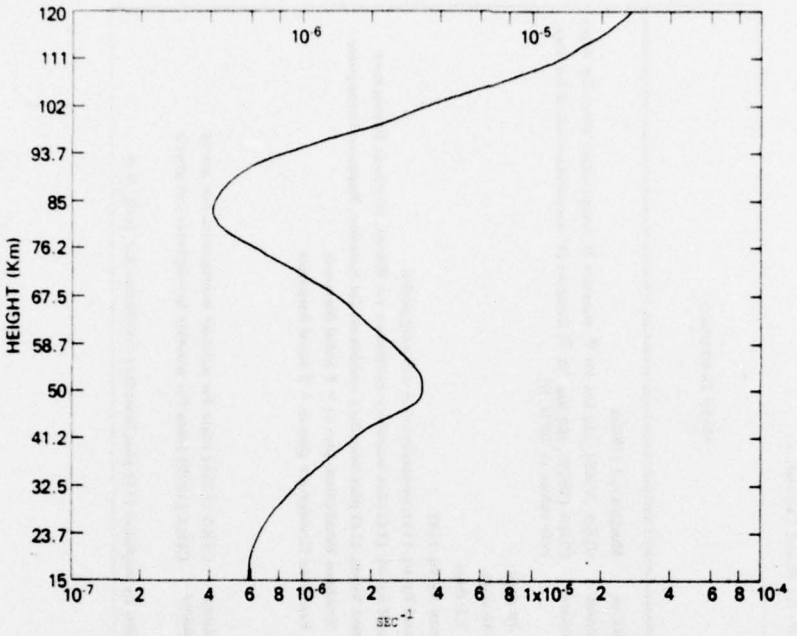

Fig. 1 – Newtonian cooling profile, $\langle\alpha\rangle$, in s^{-1}. In this and all other figures the height is the spherically averaged height of a given pressure surface.

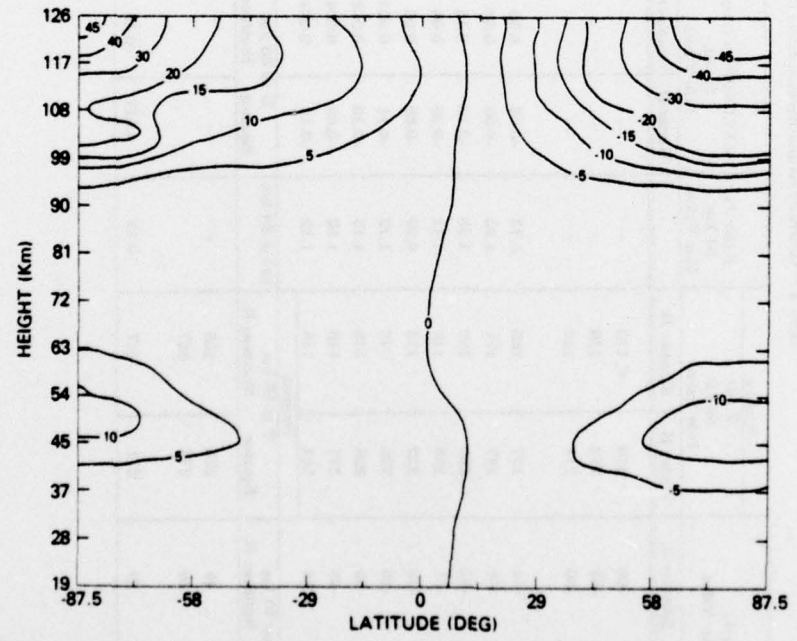

Fig. 2 – Perturbation heating rate at solstice in K day^{-1} as a function of height and latitude.

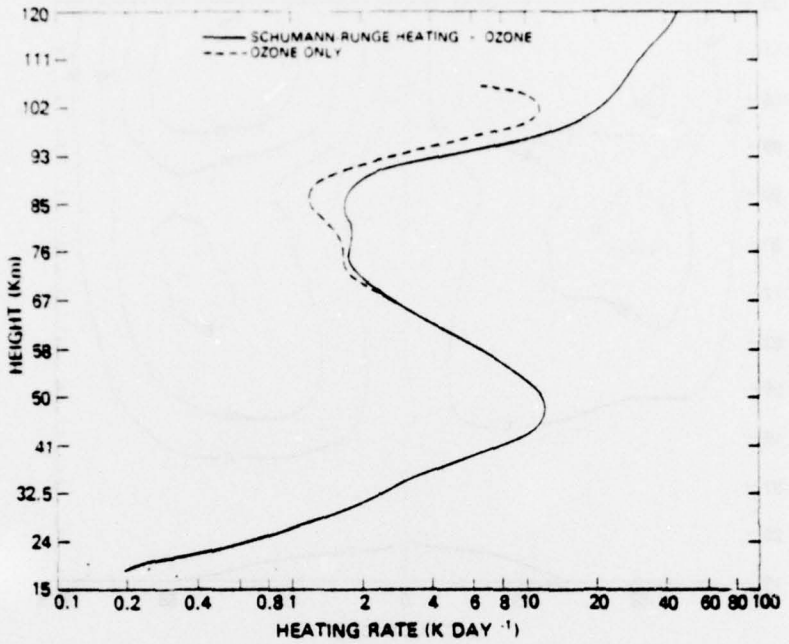

Fig. 3 – Spherically averaged heating rate as a function of altitude in K day^{-1}.

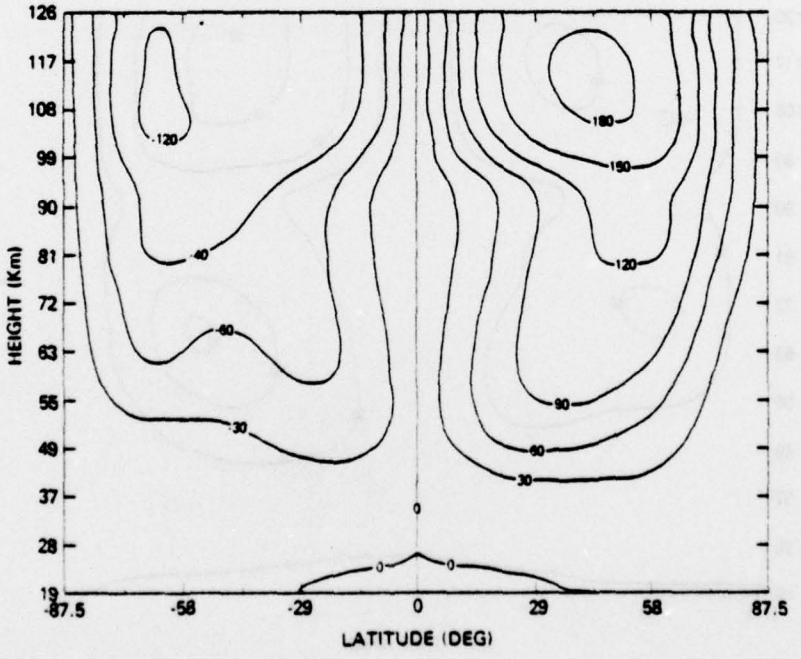

(a)

Fig. 4 – The mean zonal wind distribution computed using constant Rayleigh friction coefficients. For k_r^{-1} = (a) 30 days, (b) 15 days, (c) 7.5 days. Wind velocity is in ms^{-1}.

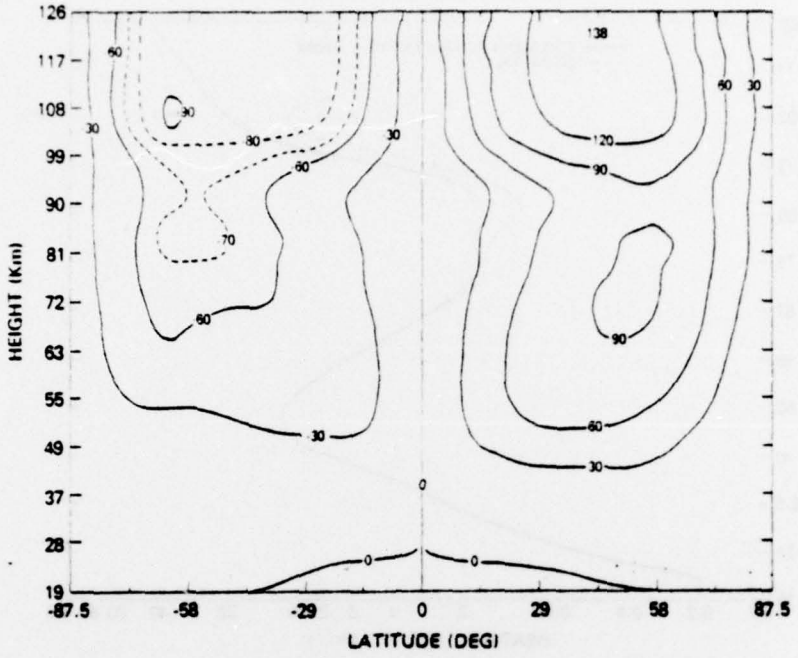

(b)

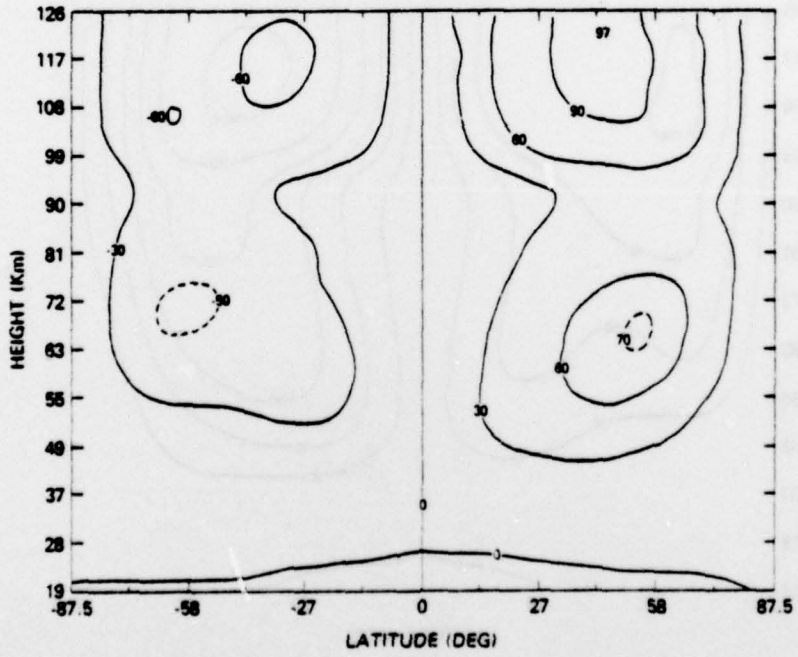

(c)

Fig. 4 – The mean zonal wind distribution computed using constant Rayleigh friction coefficients. For k_r^{-1} = (a) 30 days, (b) 15 days, (c) 7.5 days. Wind velocity is in ms^{-1}.

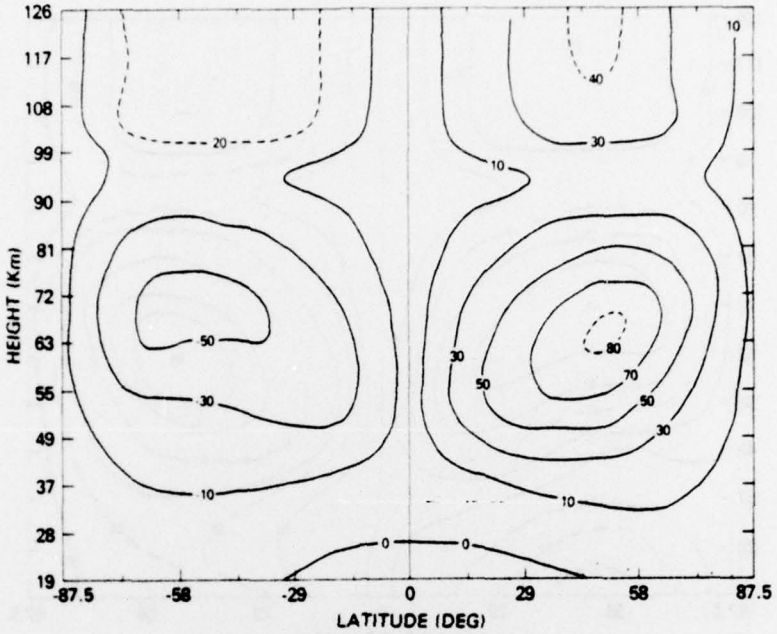

Fig. 5 – The mean zonal wind distribution computed using the Rayleigh friction profile given by equation (14).

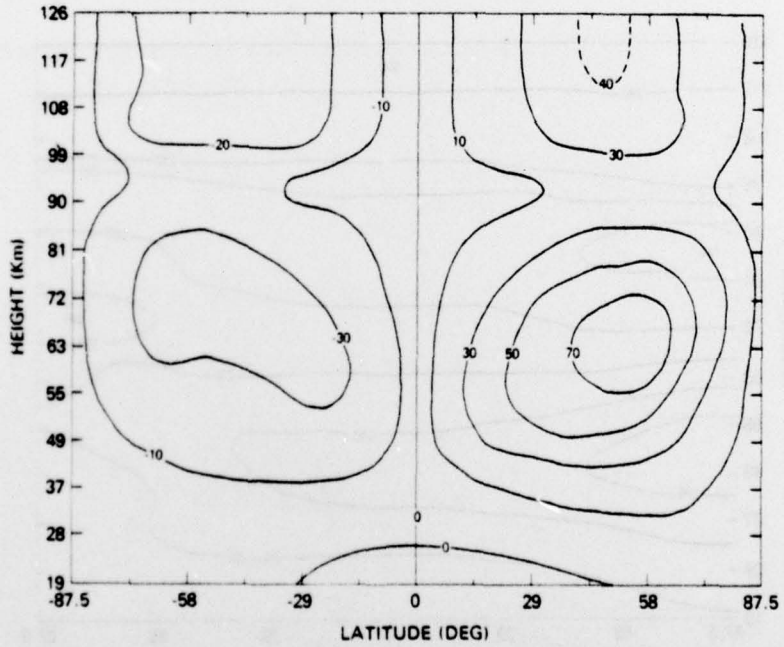

Fig. 6 – The mean zonal wind distribtution using the Rayleigh friction profile given by equation (14) and the photochemical acceleration of Newtonian cooling given by equation (12).

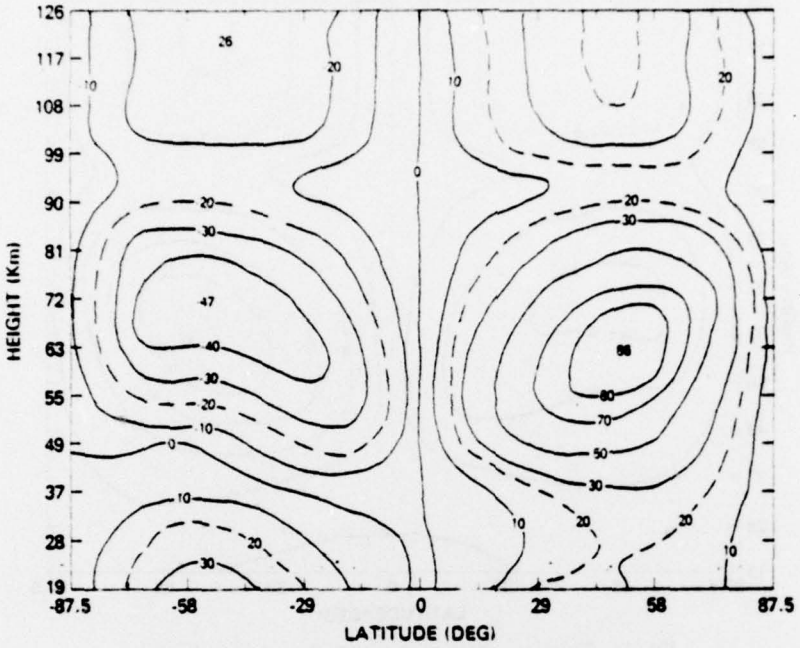

(a)

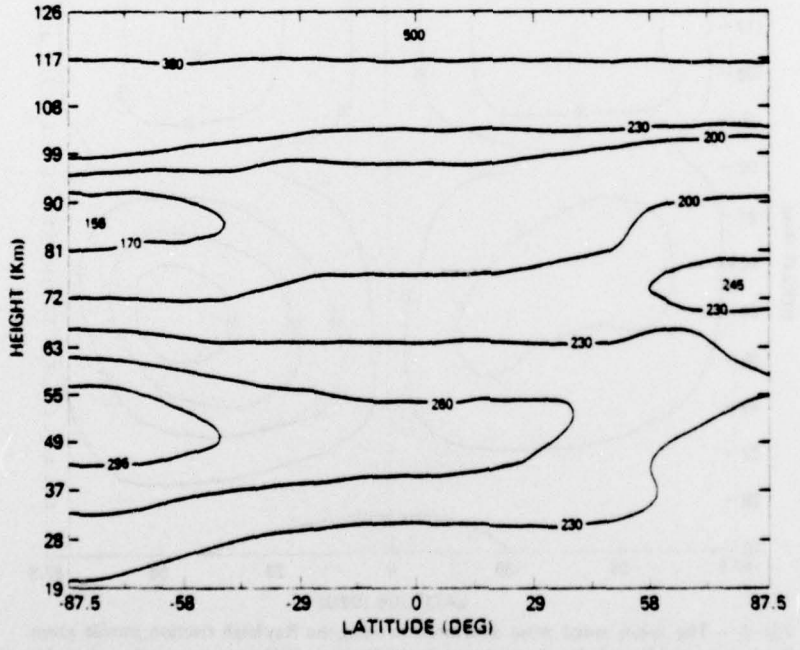

(b)

Fig. 7 – The mean zonal wind distribution computed as in Fig. 5 with the addition of tropospheric forcing for winter in the Northern Hemisphere. Part a, $\bar{u}$ (ms^{-1}); part b, $\bar{T}$(K); part c, $\bar{v}$ (ms^{-1}); and part d, $\bar{w} \times 7.0 \times 10^5$ cm (cm s^{-1}).

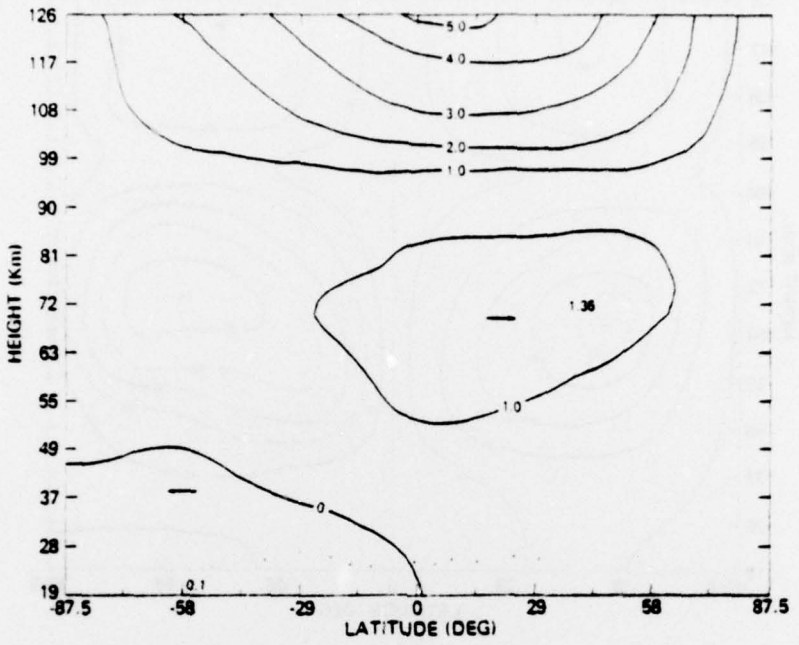

(c)

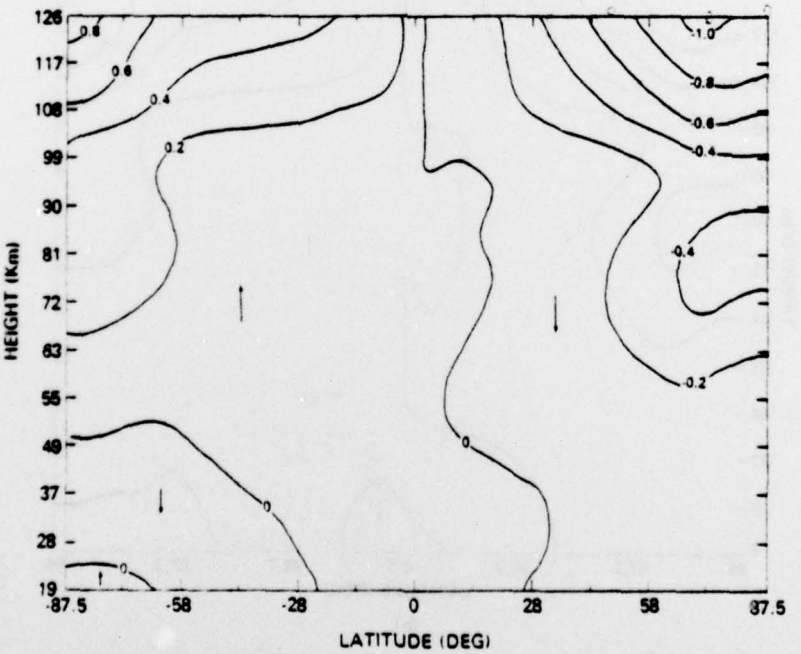

(d)

Fig. 7 – The mean zonal wind distribution computed as in Fig. 5 with the addition of tropospheric forcing for winter in the Northern Hemisphere. Part a, $\bar{u}$ (ms^{-1}); part b, $\bar{T}$ (K); part c, $\bar{v}$ (ms^{-1}); and part d, $\bar{w} \times 7.0 \times 10^5$ cm(cm s^{-1})

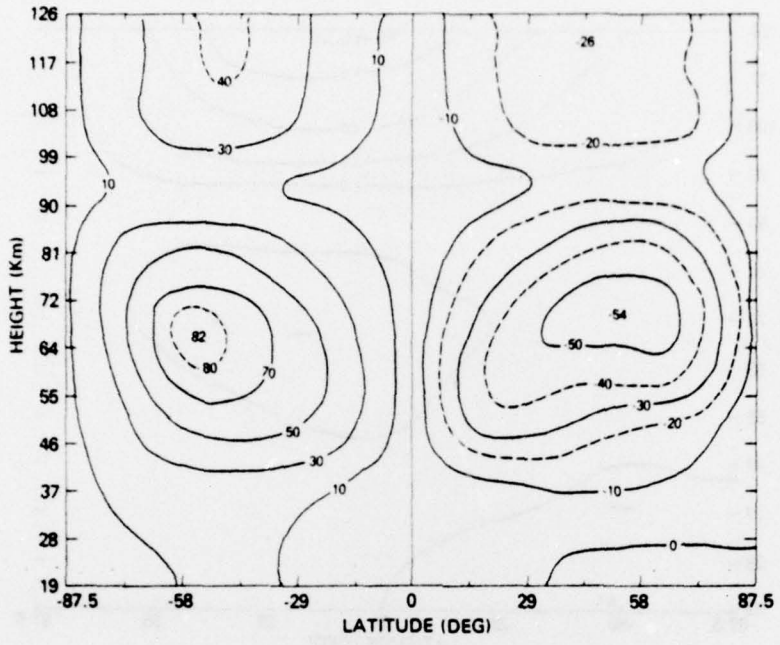

(a)

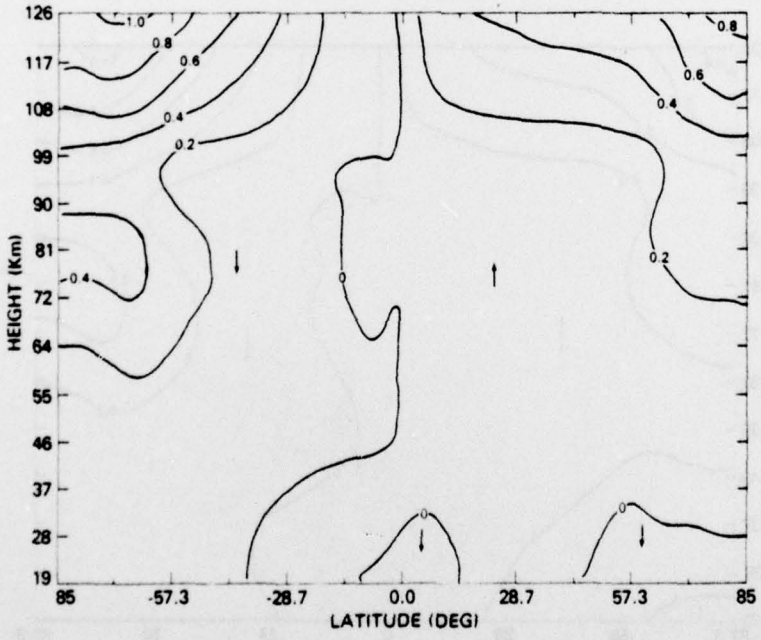

(b)

Fig. 8 – Same as Figure 8 except tropospheric forcing for summer in the Northern hemisphere is used. Part a, $\bar{u}$ (ms^{-1}); part b $\bar{w}$ ($cm\ s^{-1}$).

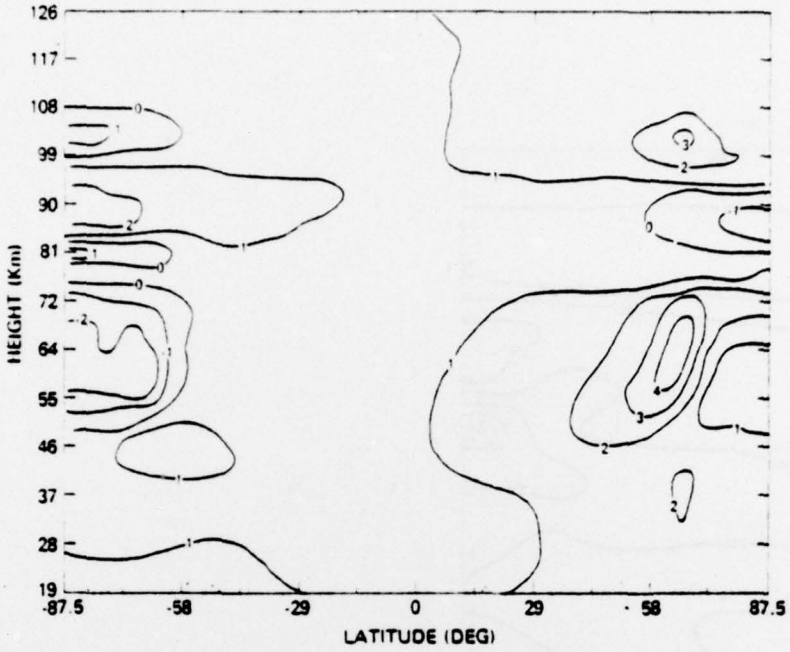

Fig. 9 – The function $\partial\bar{q}/\partial\theta \cos\theta^{-1}$ plotted for the wind profile shown in Figure 8a. Units are 1.5×10^{-4} s^{-1}).

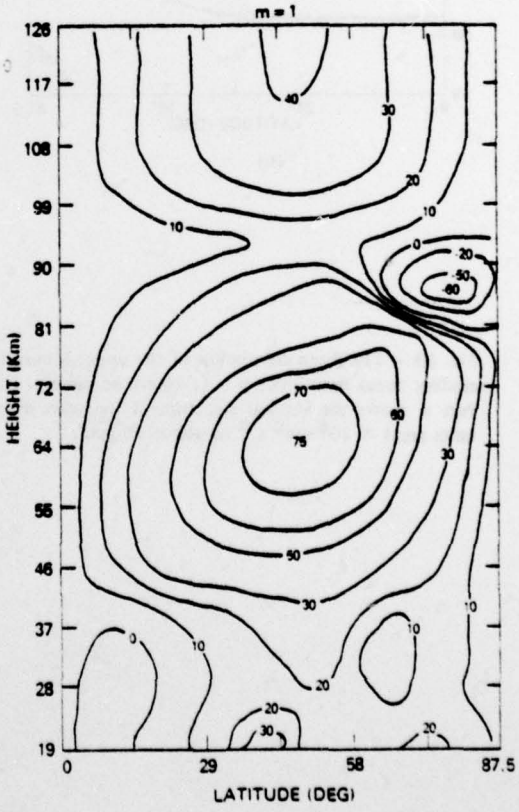

Fig. 10 – The mean circulation of the upper atmosphere including zonal harmonic, m = 1; otherwise same as Figure 8. Part e shows the vertical structure of the wave amplitude: units are 1×10^{6} cm^{2} s^{-2} or about 10 gpm.

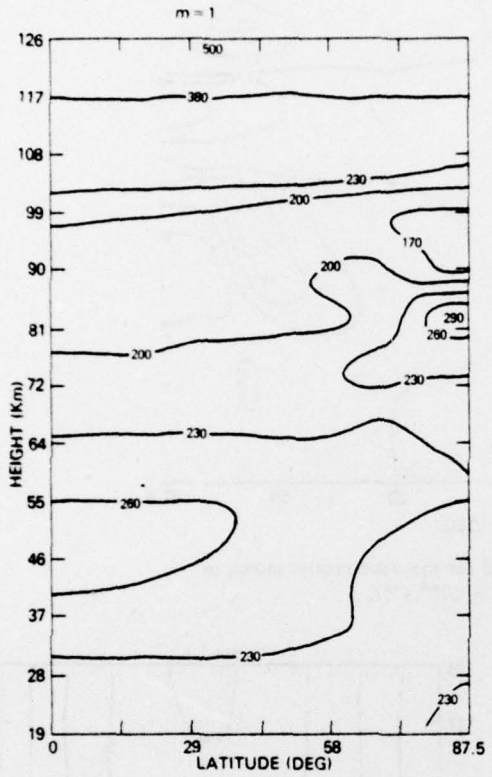

(b)

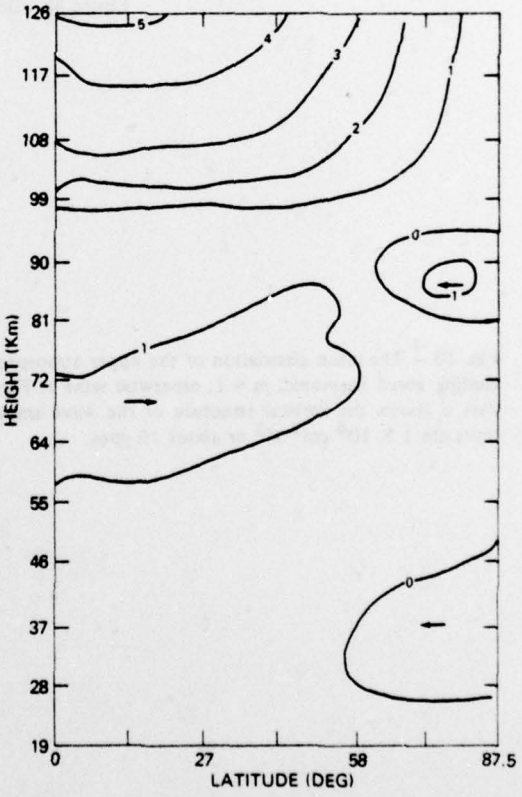

(c)

Fig. 10 – The mean circulation of the upper atmosphere including zonal harmonic, m = 1; otherwise same as Figure 8. Part e shows the vertical structure of the wave amplitude; units are 1×10^6 cm^2 s^{-2} or about 10 gpm.

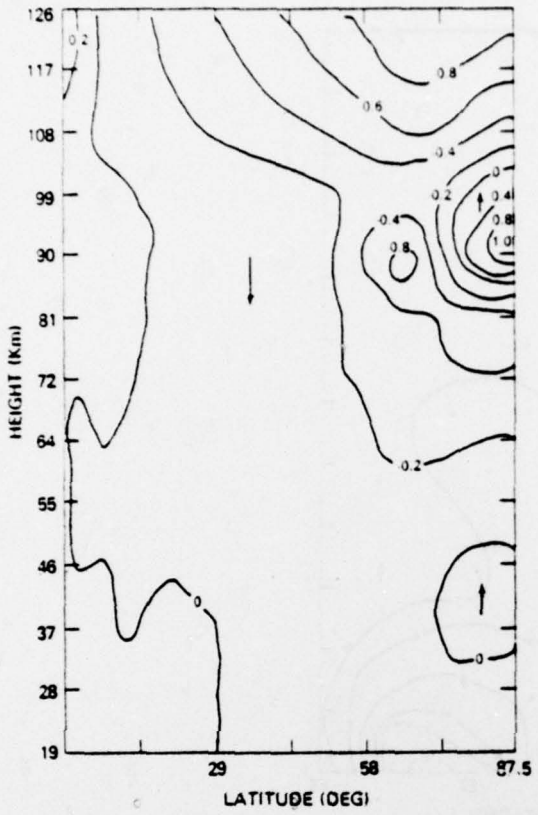

(d)

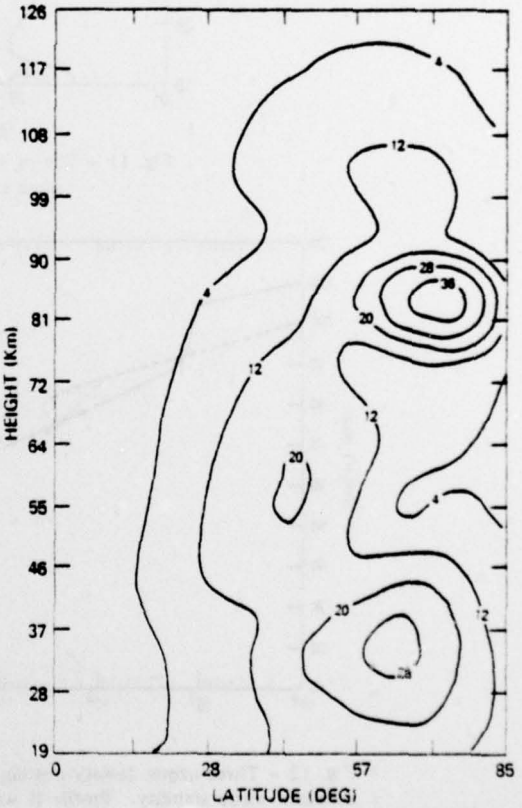

(e)

Fig. 10 – The mean circulation of the upper atmosphere including zonal harmonic, m = 1; otherwise same as Figure 8. Part e shows the vertical structure of the wave amplitude; units are 1×10^6 cm^2 s^{-2} or about 10 gpm.

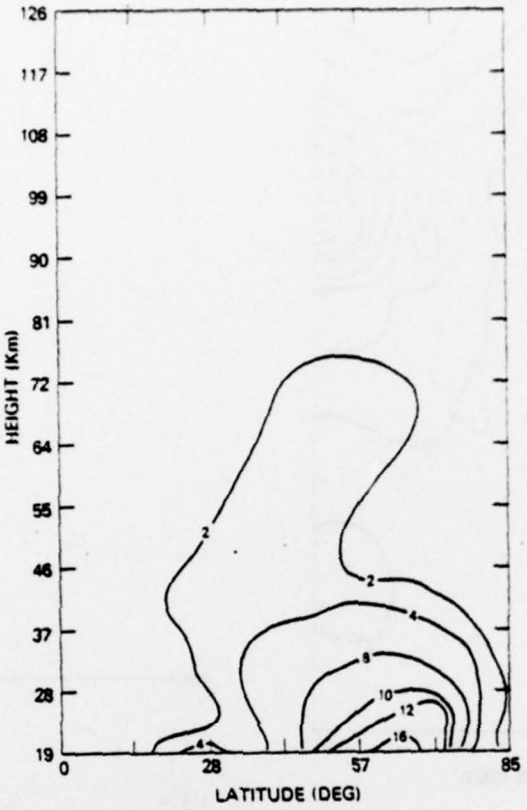

Fig. 11 – The $m = 2$ wave amplitude; units same as Figure 10e.

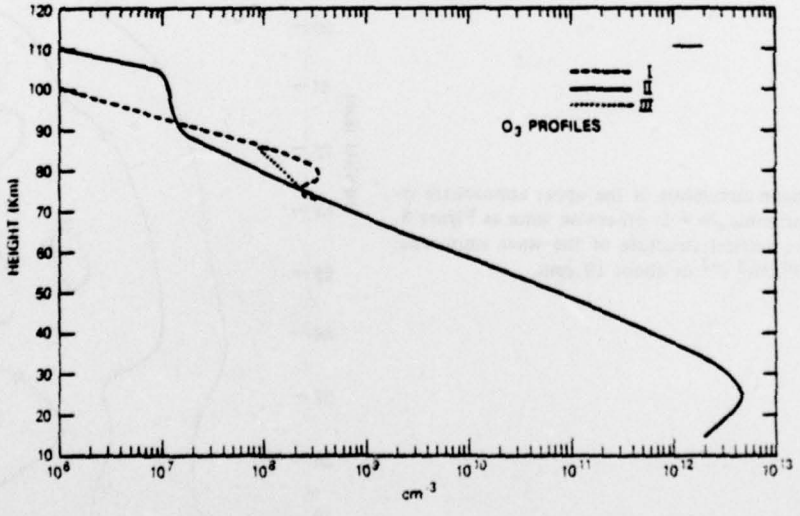

Fig. 12 – Three ozone density profiles (cm^{-3}) used to compute the heating rate and resultant static stability. Profile II was used for all calculations shown in previous figures.

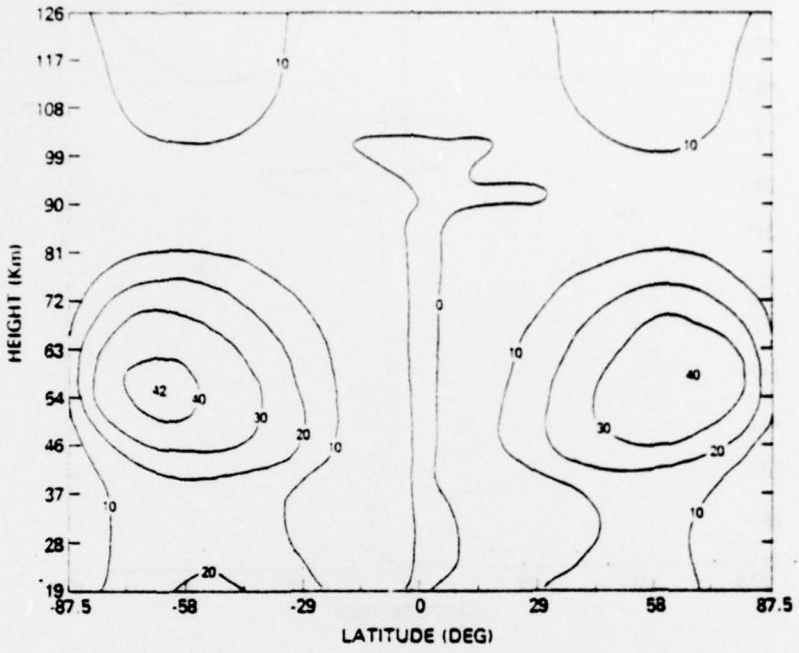

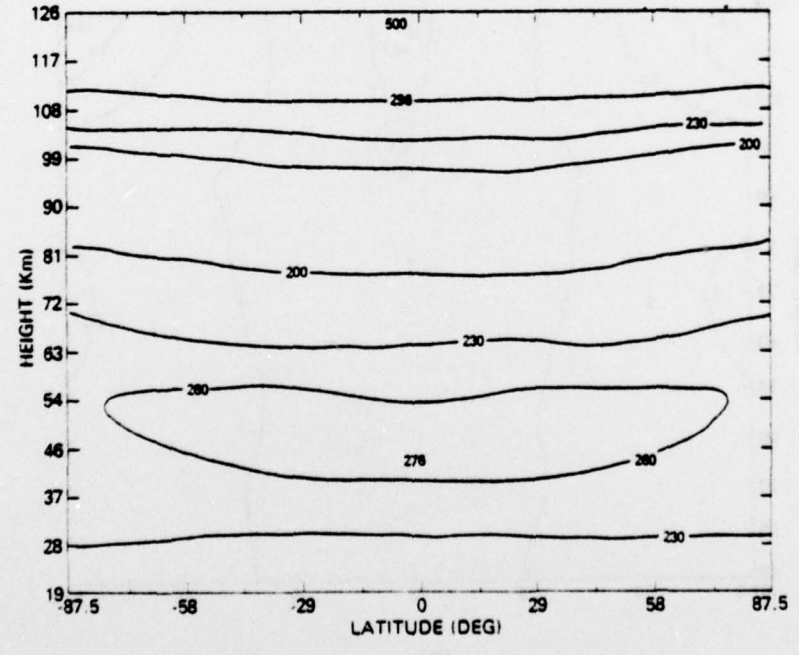

Fig. 13 – Same as Figure 7 but for equinox conditions. Part e is perturbation heating rate in K day^{-1}.

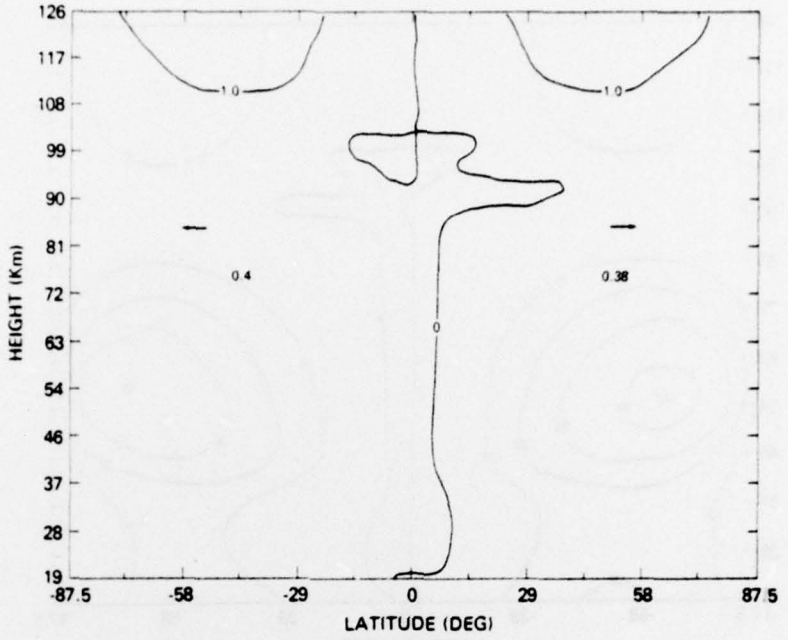

(c)

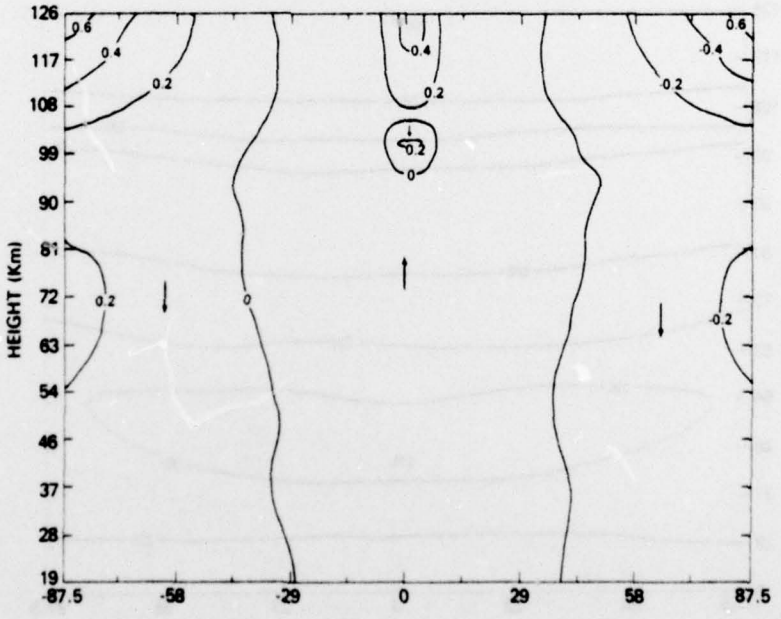

(d)

Fig. 13 – Same as Figure 7 but for equinox conditions. Part e is perturbation heating rate in K day^{-1}.

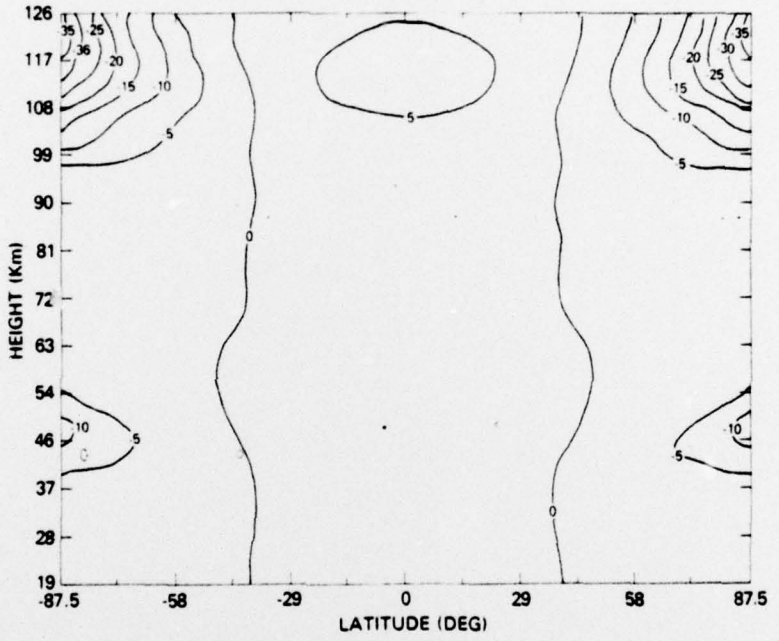

(e)

Fig. 13 – Same as Figure 7 but for equinox conditions. Part e is perturbation heating rate in K day^{-1}.

AD NUMBER ••••••••••••••••••••••••• E000063 ••••••••••••••••••••••••SCN-- A

FIELD 2: FLD/GRP(S) 04010
FIELD 3: ENTRY CLASS U

□

FIELD 4: NTIS PRICES HC MF
FIELD 5: SOURCE NAME NAVAL RESEARCH LAB WASHINGTON D C
FIELD 6: UNCLASS. TITLE THE ZONALLY AVERAGED CIRCULATION OF THE MID
FIELD 7: CLASS. TITLE
FIELD 8: TITLE CLASS. U
FIELD 9: DESCRIPTIVE NOTE INTERIM REPT.,
FIELD 10: PERSONAL AUTHORS SCHOEBERL,M. ;STROBEL ,D. ;
FIELD 11: REPORT DATE OCT 77
FIELD 12: PAGINATION 42P
FIELD 13: SOURCE ACRONYM
FIELD 14: REPORT NUMBER NRL-MR-3590
FIELD 15: CONTRACT NUMBER
FIELD 16: PROJECT NUMBER F52551
FIELD 17: TASK NUMBER WF52551713
FIELD 18: MONITOR SOURCE
FIELD 19: MONITOR SERIES
FIELD 20: REPORT CLASS U
FIELD 21: SUPPLEMENTARY NOTE
FIELD 22: ALPHA LIMITATIONS DISTRIBUTION OF DOCUMENT CONTROLLED BY NAVA
2628, WASHINGTON, DC 20375. THIS DOCUMENT I
CATALOGING INFORMATION SUPPLIED BY NRL.
FIELD 23: DESCRIPTORS •ATMOSPHERIC CIRCULATION, •COOLING, BOUNDAR
STEADY STATE
FIELD 24: DESCRIPTOR CLASS. U
FIELD 25: IDENTIFIERS •NEWTONIAN COOLING, RAYLEIGH FRICTION, SYMM
PE62759N, WUA0323
FIELD 26: IDENTIFIER CLASS. U
FIELD 27: ABSTRACT THE STEADY STATE, ZONALLY AVERAGED CIRCULAT
STUDIED WITH A QUASIGEOSTROPHIC, NUMERICAL
CONSISTENT CALCULATION OF SOLAR RADIATIVE H
FIELD 28: ABSTRACT CLASS. U
FIELD 29: INITIAL INVENTORY 0
FIELD 30: ANNOTATION
FIELD 31: SPECIAL INDICATOR
FIELD 32: REGRADING CATEGORY
FIELD 33: LIMITATION CODES 1 21
FIELD 34: SOURCE SERIAL
FIELD 35: SOURCE CODE 251950
FIELD 36: DOCUMENT LOCATION 7
FIELD 37: CLASSIFIED BY
FIELD 38: DECLASSIFIED ON
FIELD 39: DOWNGRADED TO CONF.
FIELD 40: GEOPOLITICAL CODE 1100
FIELD 41: SOURCE TYPE CODE N
FIELD 42: TAB ISSUE NUMBER 00--00

3 ••••••••••••••••••••••••••SCN-- AJN53C

MF
ESEARCH LAB WASHINGTON D C
ALLY AVERAGED CIRCULATION OF THE MIDDLE ATMOSPHERE.

REPT.,
RL,M. ;STROBEL ,D. ;
77

3590

713

UTION OF DOCUMENT CONTROLLED BY NAVAL REsEARCH LABORATORY, ATTN: CODE
ASHINGTON, DC 20375. THIS DOCUMENT IS NOT AVAILABLE FROM DDC.
ING INFORMATION SUPPLIED BY NRL.
HERIC CIRCULATION, *COOLING, BOUNDARIES, TROPOPAUSE, HEATING, RATES,
STATE

IAN COOLING, RAYLEIGH FRICTION, SYMMETRIC CIRCULATION, MIDDLE ATMOSPHERE,
N, WUA0323

ADY STATE, ZONALLY AVERAGED CIRCULATION OF THE MIDDLE ATMOSPHERE (15-125 KM) IS
WITH A QUASIGEOSTROPHIC, NUMERICAL MODEL THAT EXPLICITLY INCLUDES A SELF
ENT CALCULATION OF SOLAR RADIATIVE HEATING DUE TO O2 AND O3